DISCHARGE CHARACTERISTICS OF CMD, EMD, RHO AND SYNTHETIC BIRNESSITE IN CONCENTRATED ALKALINE ELECTROLYTE

BUQUI D. DESAI*, R. A. S. DHUME and V. N. KAMAT DALAL

Department of Chemistry, Goa University, Bambolim P.O., Santa Cruz, Goa - 403 005 (India)

(Received January 5, 1987; in revised form July 10, 1987; in final form September 28, 1987)

Summary

Different manganese dioxide polymorphs were synthesized, chemically analysed, and characterized by X-ray diffraction (XRD) and infrared (IR) spectroscopy. The MnO_2 samples were discharged in 9 M KOH at a constant current of 1 mA 0.1 g^{-1}. One of the samples, chemically precipitated MnO_2 (CMD-2), was also discharged at 2 mA and 5 mA 0.1 g^{-1}. The discharge was interrupted at specific depths of discharge and the products were removed from the test cell and characterized by XRD and IR spectroscopy as in the case of virgin samples. The oxidation state of the discharged products was $MnO_{1.75}$, $MnO_{1.68}$ and $MnO_{1.52}$, corresponding to $r = 0.5$, $r = 0.75$ and $r = 1.0$, respectively, where r is the reduction parameter. The final reduction products of 2 mA 0.1 g^{-1} and 5 mA 0.1 g^{-1} were also removed and characterized, as mentioned earlier. These products correspond to the compositions $MnO_{1.28}$ and $MnO_{0.87}$, respectively. An attempt was made to correlate the structures of these reduction products with their potentials. These results were also compared with the earlier results of Sugimori and Holton and Tye. A tentative discharge mechanism is proposed taking into consideration the different hypotheses suggested by McBreen, Sugimori, and Tye and co-workers.

1. Introduction

Several workers [1 - 20] have studied the reduction of MnO_2 and divergent results have been reported. Of these, only Bell and Huber [5], Boden *et al.* [8], Ambrose and Briggs [17], Sugimori [20], and Tye and co-workers [12] have carried out electrochemical reduction either in paper-lined cells or in test cells. Almost all of them have concentrated on electrolytic MnO_2. We have therefore attempted to determine the differences, if

*Author to whom correspondence should be addressed.

0378-7753/88/$3.50

any, between the discharge products of electrolytically deposited MnO_2 (EMD) and other polymorphs at specified depths of discharge corresponding to a particular coulombic charge.

Bell and Huber [5] reported the presence of γ-Mn_2O_3 at $MnO_{1.5}$ ($r = 1$) together with cementation of the electrode. Boden *et al.* [8] came to the conclusion that the product at $r = 1$, *i.e.*, $MnO_{1.5}$ could be either α-Mn_2O_3 or Mn_3O_4, but they were not certain about either of the two. It was Sugimori [20] who suggested the formation of Mn_3O_4 from the intermediate product, δ-MnO_2. The recent results of Tye and co-workers [21] indicate that there is a partial conversion of γ-MnO_2 to δ-MnO_2 which is then converted to Mn_3O_4 through γ-MnOOH. The oxyhydroxide potentials in alkaline medium, therefore, are not entirely representative of a γ-MnO_2/δ-MnOOH solid solution [22] in an acidic/neutral electrolyte.

In view of the above, we have attempted to characterize the discharge products, at predetermined stages of discharge, using X-ray diffractometry (XRD) supplemented by infrared (IR) spectral data. Mn_3O_4 was prepared as the reference sample following Sugimori's hypothesis that it constituted the final product of a one-electron reduction discharge.

To ensure that the reduction would be as uniform as possible (akin to a chemical reduction) we slowly discharged the test cell at 1 mA 0.1 g^{-1}.

2. Experimental

2.1. Sample preparation

The details of samples of electrolytically deposited MnO_2 (EMD), chemically precipitated MnO_2 (CMD-2), Rho-MnO_2 (ρ-MnO_2) and synthetic birnessite (δ-MnO_2) have been reported elsewhere (*J. Appl. Electrochem.*, in print) but they are summarised in Table 1. An additional sample, CMD-1, was also prepared by an identical method to that reported earlier [23] except that $KClO_3$ was used in place of $NaClO_3$. The Mn_3O_4 reference sample was prepared by heating a γ-MnO_2 sample at 1200 °C in a muffle furnace for 5 h.

2.2. Characterization of the samples by X-ray analysis

The X-ray measurements were made using Ni-filtered Cu Kα radiation ($\lambda = 1.54$ Å), scanning the samples over a range of 2θ from 10° to 90°. The operational conditions were 30 mA at 40 kV, with a step size of 0.02 and a time of 0.500 s. Graphite peaks shown in the Figures were discounted.

2.3. Infrared spectral studies

The infrared spectra were of 5 mg powdered samples dispersed in KBr pellets in the range 4000 cm^{-1} - 400 cm^{-1}. The 13 mm dia. pellets were pressed for 2 min at 8000 kg cm^{-2}.

TABLE 1

Preparation and chemical analyses data

Sample	Quantities of reagents used in the preparation	MnO_2 (%)	Mn (%)	x in MnO_{1+x}	Combined H_2O (%)	Surface area (ZIA) ($m^2\ g^{-1}$)	Tap density 200 taps ($g\ cm^{-3}$)
I.C.8	—	90.2	61.77	0.9229	2.423	79.52	1.667
CMD-1	75 g $KClO_3$ and 75 g $MnCl_2 \cdot 4H_2O$ solution	91.33	60.36	0.9563	2.928	57.75	1.470
CMD-2	65.2 g $NaClO_3$ and 75 g $MnCl_2 \cdot 4H_2O$ solution	90.93	60.02	0.9576	2.439	63.00	1.515
I.C.4	—	88.75	59.88	0.9367	2.883	50.75	2.272
EMD	500 ml of 0.5 M $MnSO_4 \cdot 4H_2O$ in 0.5 M H_2SO_4 at 95 °C. C.D. 1A dm^{-2} using Pb electrodes	88.38	59.61	0.9370	3.880	82.60	2.00
Rho	89.56 g MnO_2 + 1400 ml con.HCl at 8 °C treated 12.5 l H_2O, digested in dil. HNO_3	87.19	56.86	0.9691	4.424	148.3	1.478
Delta	150 g NaBr in 3 l H_2O with 30 ml HAC, treated 300 ml 2% $KMnO_4$. Digested in dil. HNO_3	83.67	57.68	0.9167	3.105	115.5	1.250

2.4. Density determination

(i) Pycnometric density [*24*]. This was determined using a 25 ml density bottle with kerosene at 40 °C under vacuum for 48 h.

(ii) XRD density [*25*]. The cell volume was determined from the crystallographic cell parameters a, b, c using the stoichiometric number per unit cell volume (z); the densities (D) were calculated from the relation D = Molecular weight/V_o, where

$$V_o = \frac{V \times 6.02 \times 10^{23}}{z}$$

2.5. Cell assembly

The test cell was one which had been used earlier [26] except that the zinc reference electrode was replaced by one of Hg/HgO with the cell thermostatically held at 28 °C in a water bath. The cathode mix was 0.1 g of the MnO_2 dispersed in 1 g of graphite (I.C.1) wetted with 0.5 ml of 9 M

KOH. The cathodic ingredients were thoroughly mixed and pressed in a cell at a pressure of 100 kg cm^{-2}. The discharge of the cell (normally at 1 mA 0.1 g^{-1}) was interrupted at specific depths of discharge and it was then left open circuited (OCV) for recuperation for about 8 h. The discharge was also carried out at 2 and 5 mA 0.1 g^{-1} in the case of CMD-2. The MnO_2 electrode was washed with water and dried before being subjected to X-ray diffractography and infrared spectroscopy. Two international common samples, Nos 4 and 8, were used as reference samples for electrolytically deposited and chemically precipitated MnO_2, respectively.

2.6. The manganese oxyhydroxide potentials

The potential of an Hg/HgO electrode 9 M KOH solution (*versus* SHE) at 25 °C has the following form:

$$E_R = E^\circ - 0.0296 \log a_{H_2O} - 0.0592 \text{ pH}$$

where $E^\circ = 0.926$ at 25 °C. a_{H_2O} and pH are determined from the concentration of the electrolyte, as suggested by Holton *et al.* [21]. The water activity term, $\log a_{H_2O}$, of 9 M KOH at 30 °C is −0.2932. Therefore, for Hg/HgO in 9 M KOH at 30 °C, E_r ($= E^\circ + (0.0296 \times 0.2932)$) equals 0.937. Since the temperature of our cell was 28 °C (not 30 °C) we chose 0.936 instead of 0.937, assuming E° to be 0.928 instead of 0.926 [27] (28 °C not 25 °C). The manganese oxyhydroxide potential (*versus* SHE) was obtained by adding the potential of the reference electrode, Hg/HgO, (determined by the method given above) to the potential recorded against the Hg/HgO electrode.

3. Results and discussion

The chemical analysis data are presented in Table 1. The available oxygen in all cases varies between 83.67% and 91.33%: synthetic birnessite and CMD-1, respectively. The lightly compacted (by tapping) density values (see Table 1) of I.C.4 and EMD are higher than those of the CMD samples as might be expected, but the pycnometric density values for the CMD samples (see Table 2) are slightly higher than for the EMD. These results agree with those of Holton and Tye [24]. The higher values obtained in the cases of the CMD samples are probably due to the differences in porosity/particle size of the precipitated samples.

The 'so-called' δ-MnO_2 (synthetic birnessite) was synthesized by the method recommended by Giovanoli [28], and Table 2 reveals that the XRD data are in good agreement with the ASTM values. The peak at $d = 4.93$ Å ($2\theta = 18°$), however, does not fit the pattern. We have attributed this to α-MnO_2 impurity and it is probable that the refluxing treatment with 0.5 M HNO_3 was not sufficient. Consequently, some of the Na^+ ions might have remained in the lattice to stabilize the α-MnO_2 domains and, hence, indirectly, the peak at $d = 4.93$ Å. The refluxing treatment is supposed to

TABLE 2

X-ray crystallographic and pycnometric density data

Sample	Crystal system	Lattice parameters (Å)			Cell volume V $(Å)^3$	XRD density (g cm^{-3})	Pycnometric density (g cm^{-3})
		a	b	c			
I.C.8	Orthorhombic	4.435	8.524	2.934	110.928	4.999	4.666
CMD-1	Orthorhombic	4.413	8.783	2.894	112.207	4.867	4.637
CMD-2	Orthorhombic	4.411	8.888	2.875	112.718	4.846	4.652
I.C.4	Orthorhombic	4.431	8.611	2.909	111.003	4.959	4.525
EMD	Orthorhombic	4.435	8.577	2.926	111.287	4.875	4.508
Rho	Orthorhombic	4.424	9.188	2.842	118.119	4.545	3.760
Delta	Hexagonal	2.928	2.928	7.207	53.51	5.159	3.870

produce $Mn_7O_{13}\cdot 5H_2O$ from $Na_4Mn_{14}O_{27}\cdot 9H_2O$. The discrepancy observed between the XRD density (5.159 g cm^{-3}) and the pycnometric density (3.870 g cm^{-3}), however, cannot be explained satisfactorily. The measured density is similar to that reported by Giovanoli [29] (3.66 g cm^{-3}). The X-ray characteristics of EMD are presented in Fig. 1 and are indexed on the basis of an orthorhombic unit cell (the lattice parameters and the derived XRD density are given in Table 2). The pattern obtained is almost identical to I.C.4 (Fig. 2) except for the additional, d_{042}, peak at $d = 1.22$ Å. One slight difference from the CMD pattern (shown for CMD-1 in Fig. 3 and for

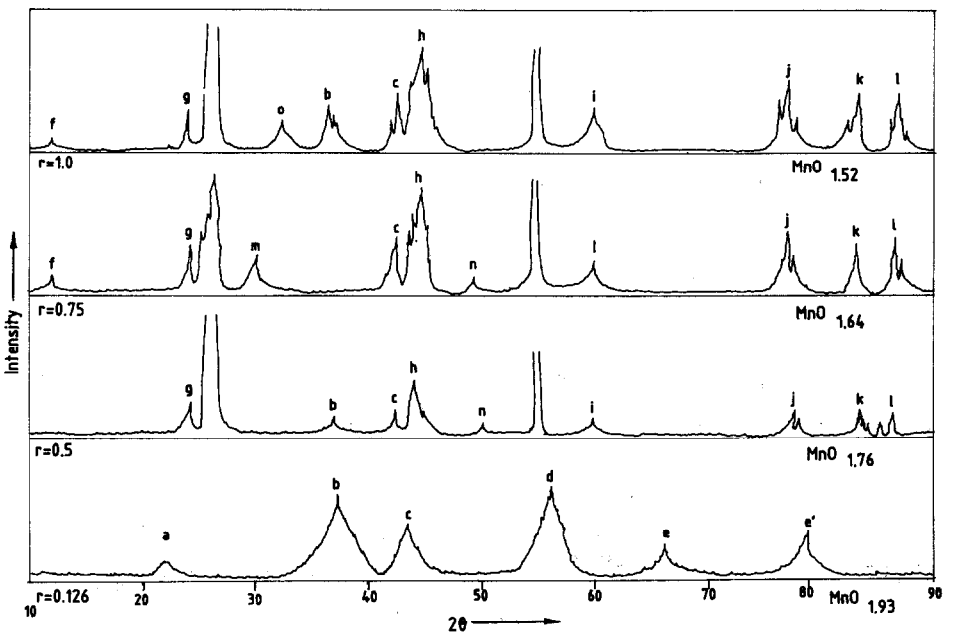

Fig. 1. X-ray diffraction pattern of EMD and its discharge products.

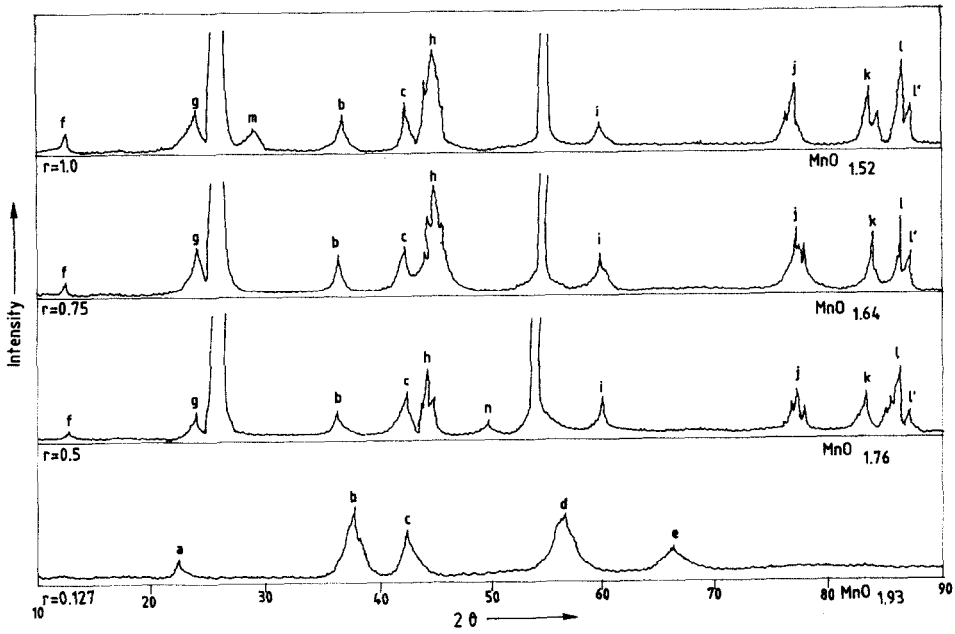

Fig. 2. X-ray diffraction pattern of I.C.4 and its discharge products.

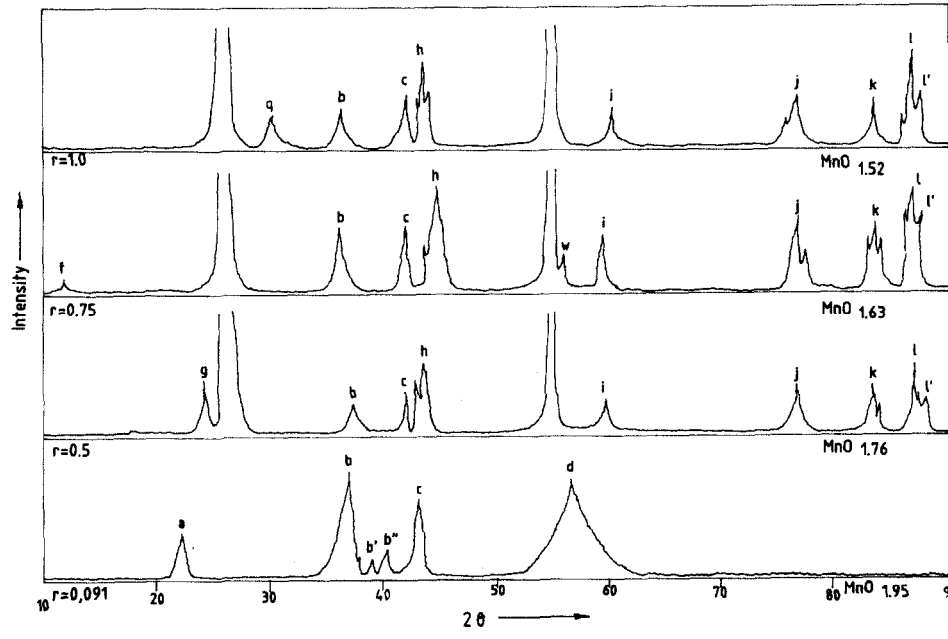

Fig. 3. X-ray diffraction pattern of CMD-1 and its discharge products.

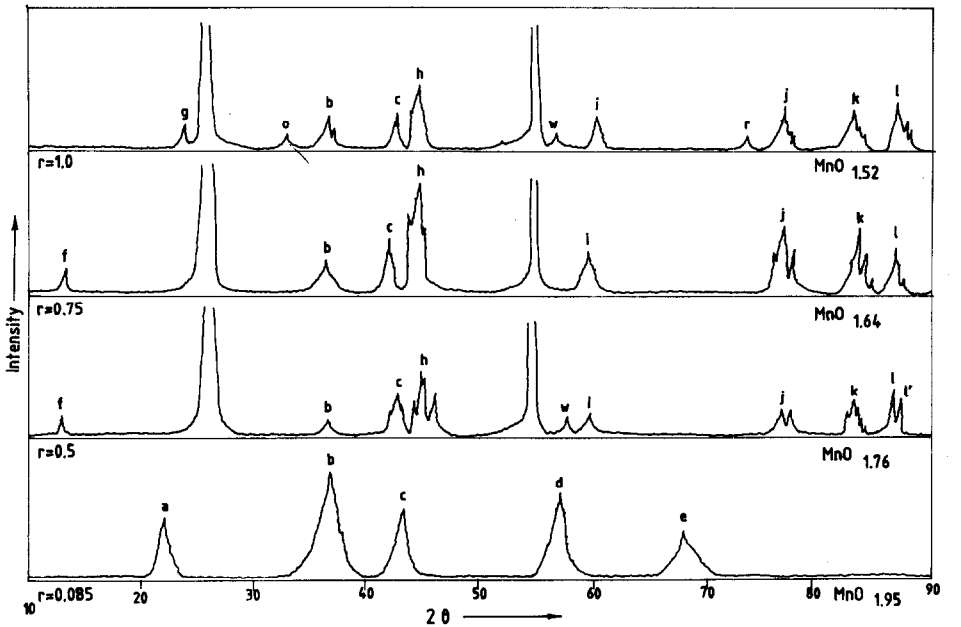

Fig. 4. X-ray diffraction pattern of CMD-2 and its discharge products.

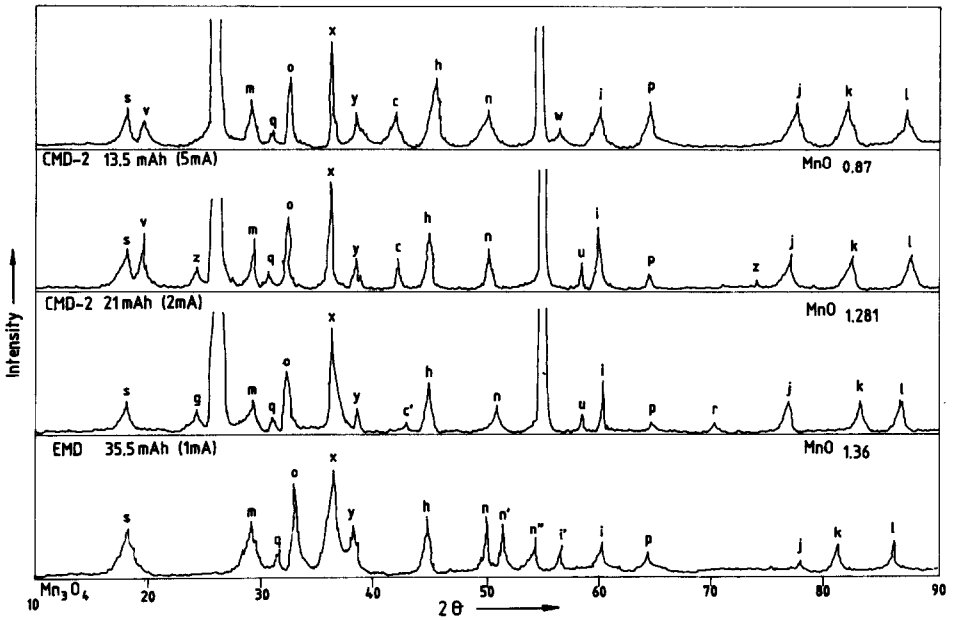

Fig. 5. X-ray diffraction patterns of the reduced products beyond $r = 1$ of CMDs, EMD and Mn_3O_4 synthesized.

CMD-2 in Fig. 4) is the nature of the d_{110} peak: in both CMD-1 and CMD-2 it is narrower. The agreement between the calculated and the observed d values is good.

The pycnometric density values for the various materials measured in kerosene at 40 °C under vacuum are presented in Table 2. These are all lower than the XRD values which are also given in Table 2 but compare favourably with reported values [29, 30]. A significant feature of the lattice parameters is the low b values which vary between 8.50 and 8.88 Å. Only in the case of Rho does the value of b appear to be 'normal' (9.188 Å). The CMD-2 prepared for these tests is analogous to one of our earlier samples (A_5) [23]. The only difference is a slight change in the relative intensities in the pattern of CMD-2 in which the "100" intensity peak is at $d = 2.42$ Å, the d_{021} peak. Our A_5 sample, on the other hand, and all of the γ-MnO_2 samples reported earlier, had shown the "100" intensity peak at $d = 1.64$ Å. Both the area and the height of the peaks yielded identical values of the relative intensities in terms of % I/I_o.

3.1. Discharge curves at different constant currents

CMD-2 was also discharged at two different constant currents, *i.e.*, 2 mA and 5 mA per 0.1 g, and the final discharge products (see Fig. 5) were similarly taken out of the test cell for characterization of the composition and the structure of the reduction products. The oxidation states were found to be $MnO_{1.28}$ and $MnO_{0.87}$, respectively (see Fig. 5). The closed circuit voltage (CCV) *versus* the state of discharge (mA h) plots are presented in Fig. 6. At 1 mA CMD-1, CMD-2 and I.C.8, all seem to follow more or less

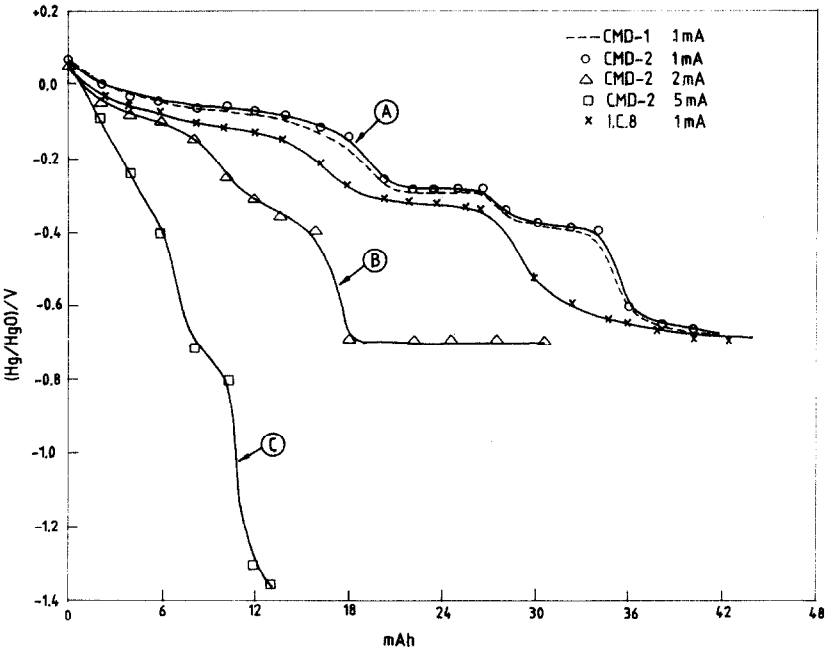

Fig. 6. Discharge curves of CMDs at different constant currents.

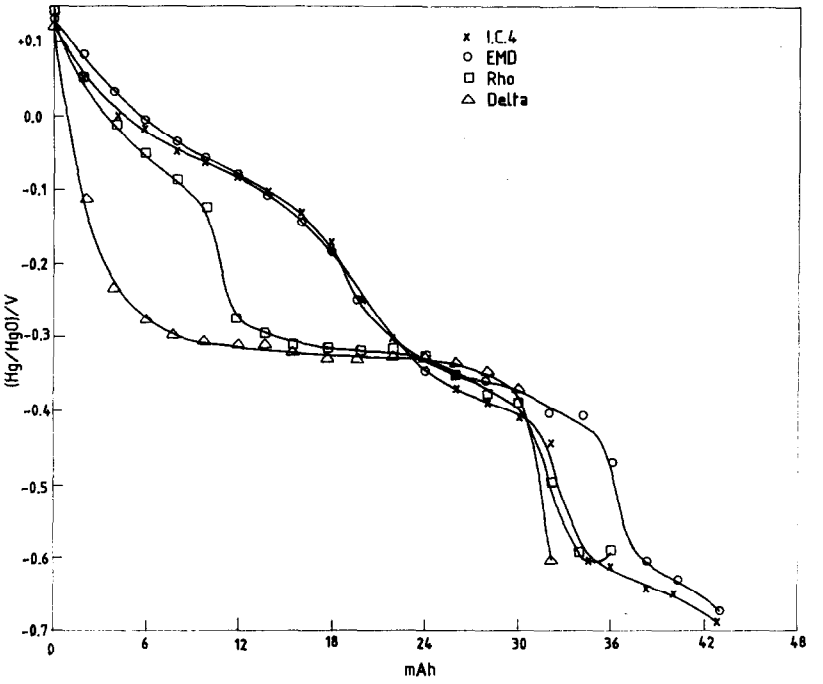

Fig. 7. Discharge curves of EMDs, Rho, Delta-MnO_2 samples at 1 mA/0.1 g.

identical discharge mechanisms. At double the current density (2 mA), however, we get a different type of curve. The beginning of the heterogeneous reaction is at 18 mA h in this case (curve 6B), which is half of that of the value, 36 mA h, when the same reaction begins at a 1 mA discharge (curve 6A). Curve 6C represents the discharge behaviour of CMD-2 at 5 mA. The observed discharge capacities agree with the theoretical values at a —0.4 V *versus* Hg/HgO cut-off voltage at all the three constant currents. The —0.4 V *versus* Hg/HgO was chosen as the cut-off voltage as this value approximately corresponds to 1 V *versus* zinc, and this is the normal cut-off voltage representing the end of one electron change.

For comparison, the discharge curves (at 1 mA, constant current) of I.C.4, EMD, Rho and Delta are presented in Fig. 7. One significant feature of CMD-1 and CMD-2 is that the discharge capacities (mA h) are substantially higher than the theoretical values while that of I.C.8 is slightly lower. In the cases of EMD and I.C.4, the one-electron reaction seems to be complete at 30 mA h, which is close to the theoretical value*. We have chosen the theoretical value of the discharge capacity as 30 mA h as an absolute standard. Since the stoichiometry of the different samples varied between 1.91 and 1.96, the theoretical values at the end of one electron

*These theoretical values were calculated using the method suggested by Atlung and Jacobsen (*Electrochim. Acta, 26* (1981) 1455).

reaction lie between 27.75 and 30.13 mA h. Rho and Delta seem to yield poor discharge capacities compared with the CMDs and EMDs at 1 mA.

In Fig. 1 the initial pattern of EMD ($MnO_{1.93}$) is presented, together with the patterns of the discharge products at $MnO_{1.76}$, $MnO_{1.64}$ and $MnO_{1.52}$, corresponding to $r = 0.5$, $r = 0.75$ and $r = 1.0$, respectively, where r is the reduction parameter in the following equation:

$$MnO_{2(1-r)} + H^+ + e^- \longrightarrow MnOOH_r$$

This figure reveals the progressive emergence of new peaks with the disappearance of the characteristic γ-MnO_2 peaks 'a', 'd' and 'c' (d values 4.01, 2.44 and 1.39 Å). New peaks which emerge are 'g', 'h', 'n', 'i', 'j', 'k' and 'l' (d values 3.75, 2.08, 1.83, 1.54, 1.24, 1.16 and 1.22 Å). Peak 'g' is a characteristic δ-MnO_2 peak which emerges at $MnO_{1.76}$. This has also been reported recently by Holton *et al.* [21] and earlier by Sugimori [20]. As the discharge proceeds further, the intensity of 'g' increases; peak 'f' ($d = 7.03$ Å), another diagnostic peak of δ-MnO_2, appears at $MnO_{1.64}$. At $r = 1.0$, however, both peaks decrease in intensity. Concurrently, the new peaks, which we attribute to Mn_3O_4, increase in intensity and become more clearly resolved. The shoulders which are seen in the peaks, 'j', 'k' and 'l' at $r = 0.5$ emerge as independent peaks at $r = 1$. Similarly, 'b' which is a 100 intensity peak of virgin $MnO_{1.93}$ decreases in intensity at $r = 0.5$, disappears at $r = 0.75$ and re-emerges at $r = 1$. This is a low intensity peak of Mn_3O_4 which occurs at $d = 2.49$ Å, *i.e.*, 36.05° 2θ. The overall pattern of this particular sample confirms the mechanism, proposed by Holton *et al.* [21], of the conversion of γ-MnO_2 to Mn_3O_4 in a strongly alkaline medium. *There could be some discrete potential ranges in which both δ-MnO_2/γ-MnOOH exist simultaneously before being converted finally to Mn_3O_4.* Giovanoli [29] has reported that γ-MnOOH is a decomposition product of δ-MnO_2, which is synthetic birnessite devoid of Na^+ ions, and having the composition $Mn_7O_{13} \cdot 5H_2O$. 2 γ-MnOOH, according to Giovanoli can also be written formally as $Mn_2O_3 \cdot H_2O$. The above mechanism is further supported by the pattern of the discharge products presented in Fig. 5. When the same EMD sample is discharged by 35.5 mA h (*i.e.*, to $MnO_{1.36}$) the resulting product reveals a pure Mn_3O_4 pattern. The discharge behaviour of CMD-1 and CMD-2 follows a similar pattern; some minor differences, however, are observed. The peak 'g' which emerges at $MnO_{1.76}$ for CMD-1 (Fig. 3) is not seen either at $MnO_{1.64}$ or $MnO_{1.52}$. Peak 'f', on the other hand, is only seen at $MnO_{1.64}$. What is significant in the pattern at $r = 1$ is the emergence of peak 'q' at $d = 3.04$ Å, not shown by CMD-2 (Fig. 4) which exhibits a peak 'o' ($d = 2.74$ Å) instead. CMD-2, at $r = 1$, also exhibits additional peaks 'w' and 'r' at $d = 1.63$ Å (Mn_3O_4) and $d = 1.28$ Å which are not seen in either CMD-1 or EMD (Fig. 1) at $r = 1$. The characteristic peak 'g' of δ-MnO_2 appears at $r = 1$ in CMD-2 but, surprisingly, not at $r = 0.5$ (Fig. 4). This "hide-and-seek" behaviour of peaks 'g' and 'f' in the cases of CMD-1 and CMD-2 appears to be due to the intermediate δ-MnO_2 of higher disorder and dispersion [31]. It is probable that this is more pronounced in CMDs due to the presence of

either K^+ and/or Na^+ ions. The pattern of the synthetic birnessite discharge products retains 'g' and 'f' peaks from $r = 0.5$ to $r = 1$. These peaks disappear only with deeper discharges, *i.e.*, beyond $r = 1$ or at a higher current density. It can therefore be concluded that the discharge mechanism of CMD-1, CMD-2 and I.C.8 (see Fig. 8) is slightly different in terms of the composition of the oxyhydroxides formed between $MnO_{1.76}$ and $MnO_{1.52}$. There is some indication of this effect in the infrared spectroscopy (see discussion below). One could also explain the appearance and disappearance of the δ-MnO_2 lines on the basis of the following tentative hypotheses:

(i) the amount of δ-MnO_2 formed is very small;

(ii) δ-MnO_2 is formed only on the surface;

(iii) the amount formed on the surface of oxyhydroxide particles is more accessible to X-rays.

The conversion of δ-MnO_2 to γ-MnOOH is not clearly observed, as the 'characteristic peaks' of γ-MnOOH [21] (at d values 1.77, 2.20, 2.28 and 2.64) are not seen either at $r = 0.5$ or at $r = 1$ in any of our samples. The conversion of δ-MnO_2 to Mn_3O_4 is not complete even at $r = 1$ in almost all the samples. The complete disappearance of the δ-MnO_2 phase occurs at a much lower oxidation state, *i.e.*, $MnO_{0.87}$ (see Fig. 5). Before this particular lower oxidation stage is reached, almost all discharge products display a mixed pattern of δ-MnO_2 and Mn_3O_4. Further, the peak in the neighbourhood of 4 Å, reported by Holton and Tye (a δ-MnOOH peak according to them), is not seen in any of the discharge products investigated here. On the other hand the peak at $d = 3.50$ Å, a typical δ-MnOOH peak, is displayed only by the discharge products of synthetic birnessite (δ-MnO_2) at $r = 0.5$ and $r = 0.75$ (see Fig. 9). Surprisingly, this peak disappears at the next oxidation stage at $r = 1$. Whereas Holton *et al.* [21] reported the appearance of a 100 intensity Mn_3O_4 line ($d = 2.49$) at $MnO_{1.68}$, in our samples it appears at $MnO_{1.75}$ itself. There is, of course, the possibility of the 100 intensity γ-MnOOH line ($d = 3.4$ Å) being masked by the strongest graphite peak. Finally, there is tenuous evidence of the separator paper turning pink at $r = 1$. This was also reported by Sugimori [20] and is further confirmed from the pattern displayed by the δ-MnO_2 itself as its own reduction products (see Fig. 9) continue to show peaks 'f' and 'g' even at $r = 1$. Several workers [5, 8, 9, 17, 20, 21] have reported Mn_3O_4 as a reduction product of γ-MnO_2 in alkaline electrolyte.

We suggest that the formation of Mn_3O_4 may be:

$$\gamma, \delta\text{-}MnO_2 \longrightarrow \delta\text{-}MnO_2/\gamma\text{-}MnOOH \longrightarrow \gamma\text{-}MnOOH, HMnO_2^- \longrightarrow Mn_3O_4$$

where γ, δ-MnO_2 refers to the virgin polymorphs, *i.e.*, before discharge. The mechanism given above indicates that γ-MnO_2 changes to δ-MnO_2 which, in turn, changes to γ-MnOOH and then, finally, to Mn_3O_4.

The conclusion that the Mn^{3+} ions are the intermediates in the conversion of γ–δ-MnO_2 [20] seems to be valid as far as this work is concerned.

Even the ρ-MnO_2 seems to get converted to Mn_3O_4 via δ-MnO_2 (see Fig. 10). Since the particle size is very small (surface area = 148.3 $m^2 g^{-1}$) it

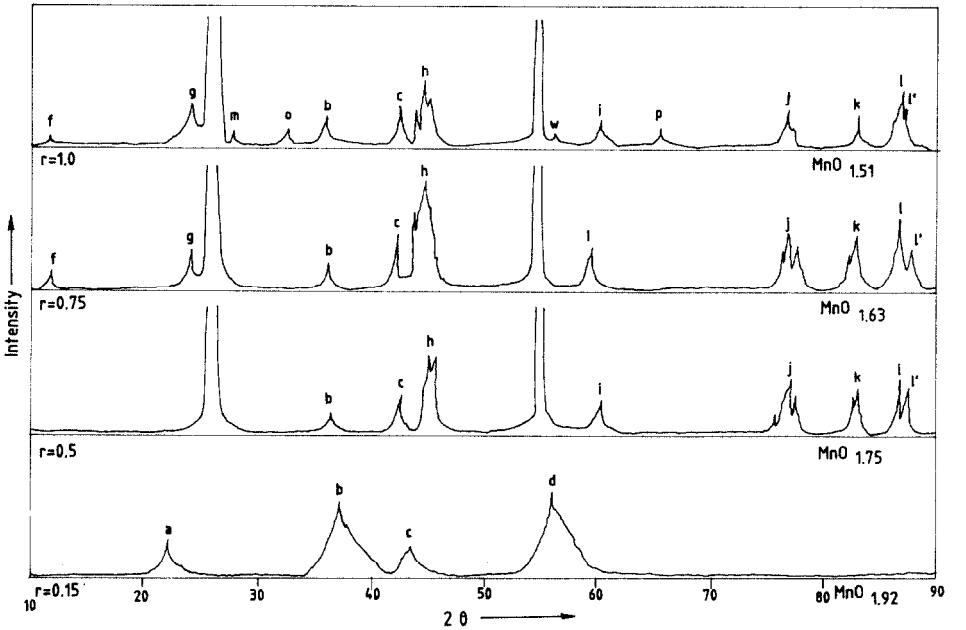

Fig. 8. X-ray diffraction pattern of I.C.8 and its discharge products.

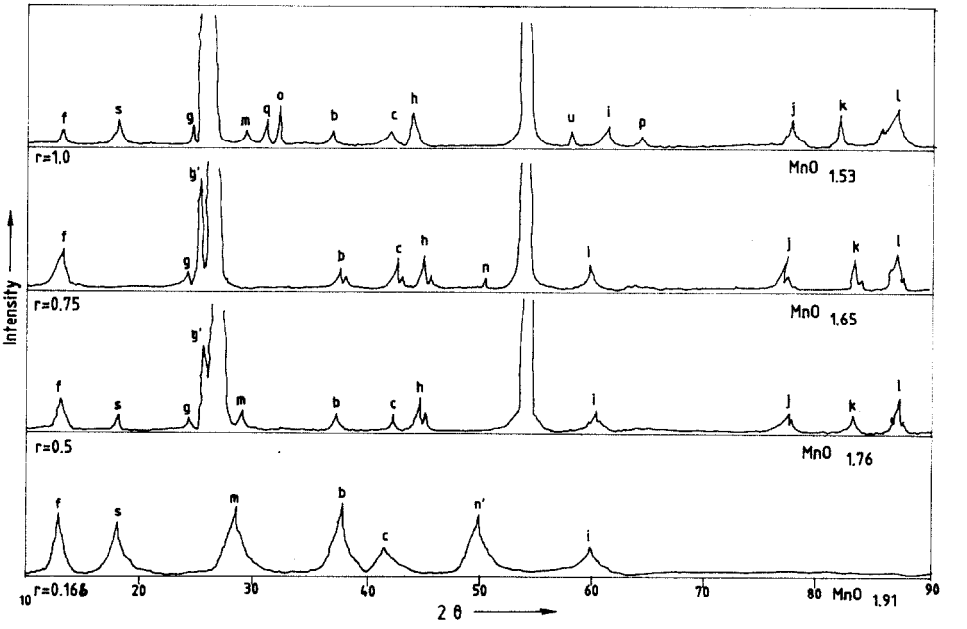

Fig. 9. X-ray diffraction pattern of δ-MnO_2 and its discharge products.

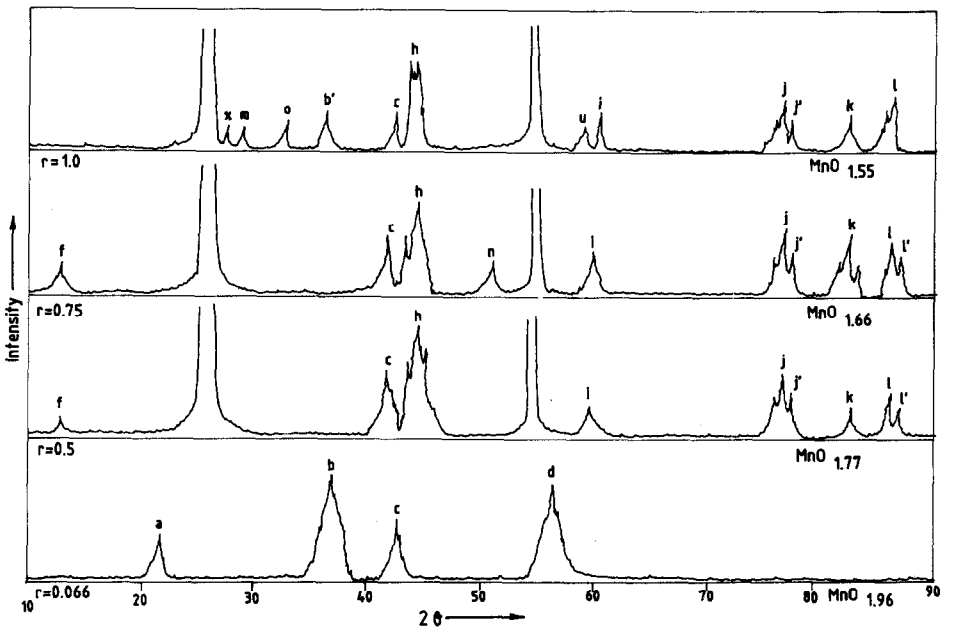

Fig. 10. X-ray diffraction pattern of ρ-MnO_2 and its discharge products.

is probable that the thin platelets of δ-MnO_2 formed do not affect the incident X-rays. Otherwise, the product at $r = 1$, corresponding to $MnO_{1.55}$, exhibits a pattern almost identical to the other patterns at the same state of discharge.

In summary, there is practically no difference in the final discharge products of EMD and CMD. Even the final product of synthetic birnessite shows only a minor variation in the line intensities. The end product, in almost all cases up to $MnO_{0.87}$, seems to be Mn_3O_4 and nothing else (see Table 3).

We have also calculated the lattice parameters and the cell volumes of the discharge products below $MnO_{1.5}$. The ratio of these volumes per unit of reduction *versus* the degree of reduction X are plotted in Fig. 11, which reveals the formation of a new phase from $MnO_{1.5}$ onwards.

It has already been established that the reduction products of γ-MnO_2 undergo Jahn–Teller distortion in acidic/neutral electrolytes [15, 32, 33]. The distortion is expressed as the ratio of two edges of an octahedron, a″/a′, where:-

$$a'' = \frac{1}{2}\left(\frac{b^2}{4} + c^2\right)^{1/2} \text{ and } a' = c$$

An attempt was therefore made to find out if the reduction products of MnO_2 in alkaline medium also undergo this distortion. The values of a″/a′

TABLE 3

X-ray powder diffraction data of the oxides of manganese

Mn_3O_4 ASTM 24 - 734		Mn_3O_4 synthesized			Reduction product $MnO_{0.87}$		
d (Å)	I/I_o	2θ	d (Å)	I/I_o	2θ	d (Å)	I/I_o
4.924	40	18.4	4.8216	40	18.0	4.9279	40
3.089	40	29.3	3.0480	50	19.1	4.6465	30
2.881	17	31.3	2.8577	20	29.0	3.0789	36
2.768	85	32.6	2.7466	87	30.9	2.8938	10
2.487	100	36.4	2.4682	100	32.4	2.7631	70
2.463	20	38.3	2.3500	40	36.1	2.4880	100
2.367	20	44.7	2.0273	40	38.1	2.3618	30
2.0369	20	50.1	1.8207	60	42.3	2.1365	25
1.8286	20	51.00	1.7006	40	44.5	2.0359	45
1.7488	25	54.2	1.6922	30	50.7	1.8005	30
1.7008	10	56.4	1.6313	18	56.1	1.6393	20
1.6405	8	60.1	1.5395	20	59.9	1.5441	37
1.5445	50	64.3	1.4487	15	64.5	1.4467	40
1.4405	20	77.6	1.2306	10	77.5	1.2316	35
1.2305	5	80.72	1.1903	10	83.6	1.1566	30
1.1978	5	85.90	1.1314	10	87.2	1.1168	30
1.1245	8						
1.0826	8						

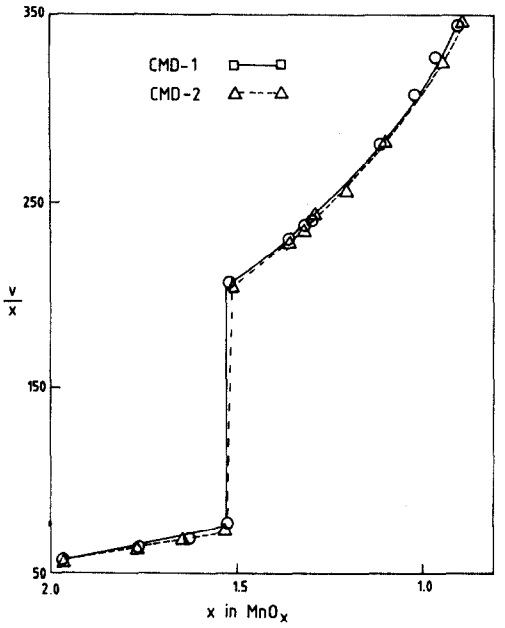

Fig. 11. Variation of the ratio of cell volume to the degree of reduction as a function of the degree of reduction.

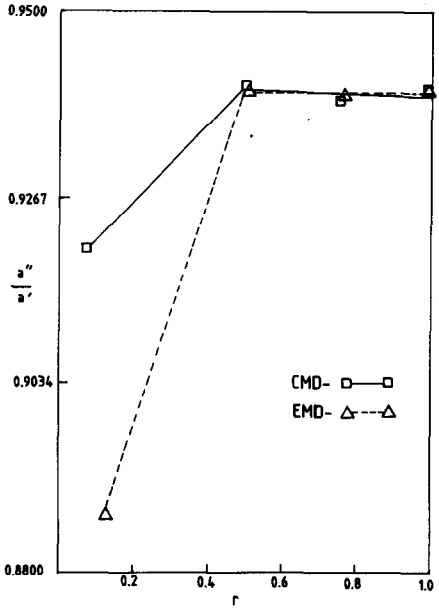

Fig. 12. Ratio of the octahedron cell edges *vs.* *r*.

as a function of r are plotted in Fig. 12. No such distortion appears to be occurring in the range $r = 0.5$ to $r = 1$. The ratios of the two edges of an octahedron remain more or less constant from $r = 0.5$ to $r = 1$. These ratios, however, show an abrupt increase from that of virgin MnO_2 to that at $r = 0.5$. It will also be noted from Fig. 12 that these values (0.88 - 0.90) are lower than those reported by Maskell *et al.* (1 - 1.1) [33]. This is due to the overall decrease in the lattice parameter b, not only in the case of our samples, but also in I.C.4 and I.C.8. This structural behaviour could be construed as supporting evidence for the dynamic equilibrium between Mn^{3+} in solution and γ-MnO_2 solid solution. The greater solubility of Mn^{3+} ions in the strongly alkaline medium may also be responsible. The Mn^{3+} ions, which are formed as a result of electrochemical reduction, are either dissolved in 9 M KOH or they participate in the partial conversion of γ-MnO_2 to δ-MnO_2. In brief, it appears that no phase having Mn^{3+} ions is stable in the solid state in the range $r = 0$ to $r = 0.8$ (where r_o is the amount of initial inactive MnOOH present in the virgin material).

It is interesting to note the potential changes that occur between $r = 0.7$ and $r = 0.8$ and from $r = 0.8$ to $r = 1$ or even beyond (see Figs. 6, 7). The potentials drop abruptly from about $r = 0.65$ to $r = 0.8$ ($MnO_{1.62}$) and then remain more or less constant. Holton *et al.* [21] proposed the following reaction to account for this behaviour:

$$3MnOOH + e^- \rightleftharpoons Mn_3O_4 + H_2O + OH^-$$

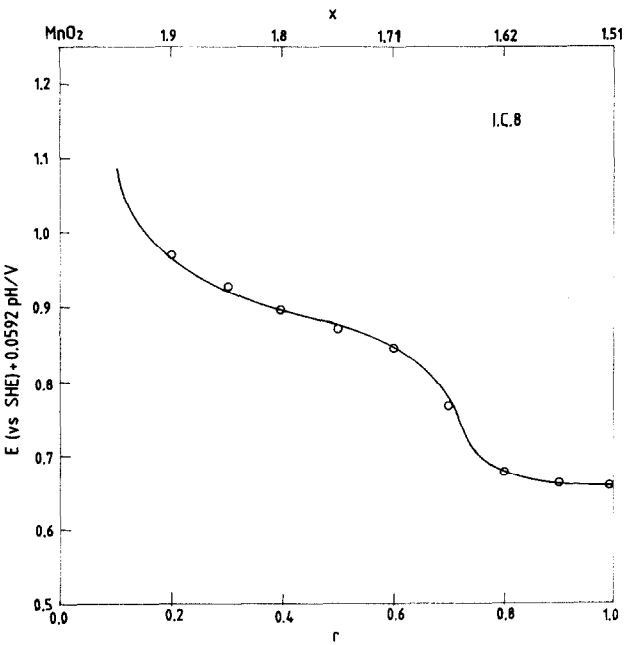

Fig. 13. Plot of E(*vs.* SHE) + 0.0592 pH *vs.* r.

Using G° values of −134.6, −306 and −56.69 kcal mole^{-1} for MnOOH, Mn_3O_4, and H_2O, respectively, they found that $E_{(SHE)}$ + 0.059 pH for the above reaction is 0.7 V. We are unable to obtain this value of $E_{(SHE)}$ + 0.059 pH from our observed curves. If, however, McBreen's reaction scheme is used instead, then we get a value of 0.62 V (see Fig. 13 which is from our earlier publication) for $E_{(SHE)}$ + 0.059 pH. His reaction is as follows:

$$2MnOOH + HMnO_2^- \longrightarrow Mn_3O_4 + H_2O + OH^-$$

Using the G° values of −120.9 kcal mole^{-1} for $HMnO_2^-$ and −134.6 kcal mole^{-1} for MnOOH, the calculated potential is 0.62 which, in terms of our representation here, becomes equal to −0.313 V *versus* Hg/HgO. Our discharge curves (see Figs. 6, 7) clearly exhibit the almost flat potential range from −0.32 V *versus* Hg/HgO onwards (*i.e.*, 0.613 in terms of $E_{(SHE)}$ + 0.059 pH). McBreen's hypothesis appears, therefore, to hold good at this stage of the electrochemical reduction in case of I.C.4, CMD-1 and CMD-2.

3.2. Infared spectral data

Infrared spectroscopy has often been used as a useful supplementary tool to X-ray for the characterization of the manganese oxide system [34]. Our earlier attempt [35] also prompted us to study the discharge products by infrared spectroscopy which has the additional advantage of being a sensitive tool for disordered structures.

Figures 14, 15, 16 reveal that CMD-1, CMD-2, EMD and I.C.4 have common absorption frequencies between 500 and 510, 545 and 550, 495 and 600 and 670 cm^{-1} from the starting substance to the final product at $r = 1$. The broad, but weak bands between 1600 and 1700 cm^{-1} and 3200 and 3600 cm^{-1}, representative of bending and stretching modes of water, are not shown by EMD, I.C.4 and CMD-2 beyond $r = 0.5$. They are indicative of the presence of small amounts of water, which does not occupy well-defined crystallographic sites [34]. The low intensity of these is also indicative of a lower order of crystallinity.

There are, however, some curious features of the discharge products which are difficult to interpret. One of them is the absence of the peaks between 1600 and 1700 cm^{-1} and between 3200 and 3600 cm^{-1}. If γ-MnOOH were the intermediate product then these absorption frequencies should have appeared in the reduced products of composition $MnO_{1.75}$ and $MnO_{1.68}$, or thereabouts. Even if OH were to occupy crystallographically distinct sites then a sharp absorption band near 3400 cm^{-1} should have occurred [34], but this is not the case. It appears, therefore, that OH groups in γ-MnOOH are not free either to bend or to stretch, *i.e.*, their bending and stretching modes of vibration are quenched. (No IR data of pure γ-MnOOH

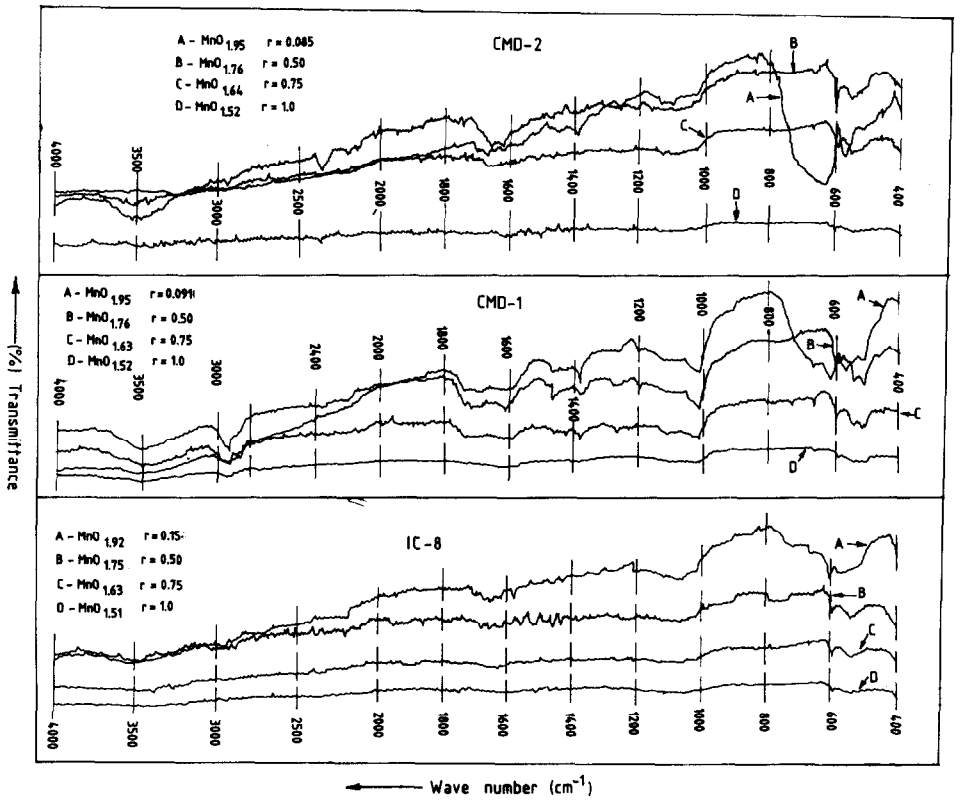

Fig. 14. Infrared spectra of CMDs and their discharge products.

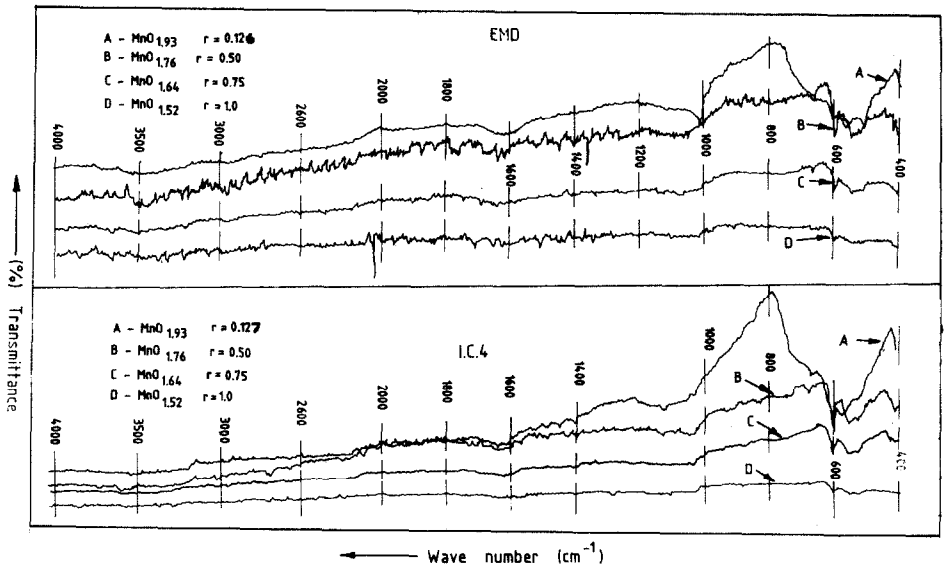

Fig. 15. Infrared spectra of EMDs and their discharge products.

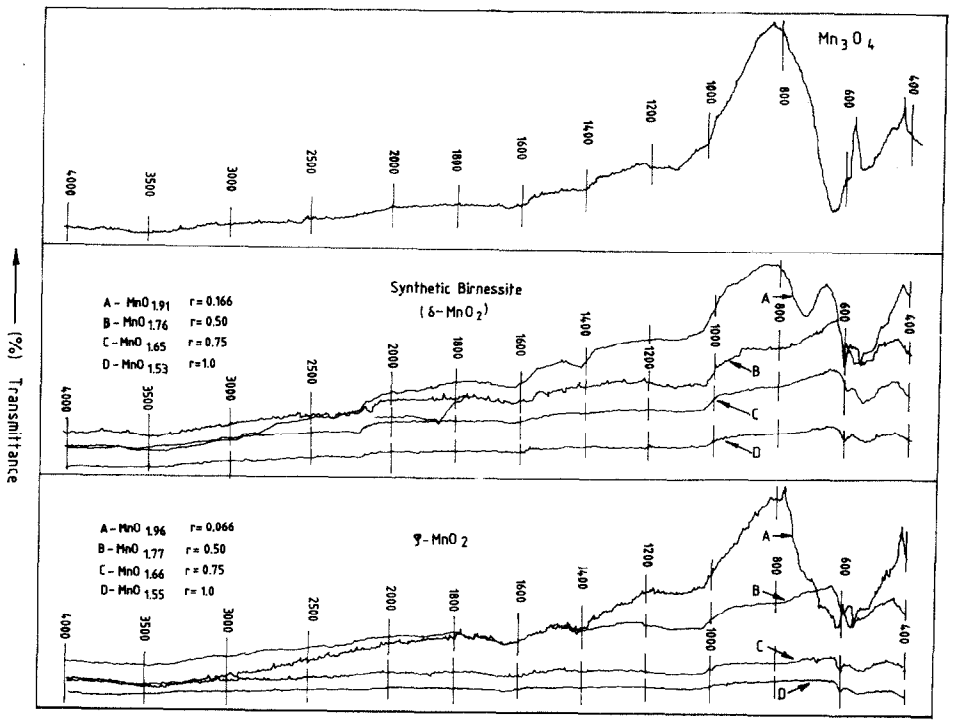

Fig. 16. Infrared spectra of Mn_3O_4, Rho and Delta and discharge products of ρ- and δ-MnO_2.

were available for comparison.) It is only the discharge products of CMD-1 which exhibit both these features right up to $r = 0.75$, but even in this case only the stretching mode (rather weak) is exhibited at $r = 1$. The absence of both the bands at $r = 1$ is understandable as at this stage the nucleation of Mn_3O_4 is well advanced.

The only evidence — rather tenuous — for the presence of γ-MnOOH is the weak absorption band between 1020 and 1040 cm^{-1} which is shown by I.C.4 and CMD-1. EMD and CMD-1 exhibit it only up to $MnO_{1.75}$ and no further.

These results are in general conformity with the X-ray data which do not indicate a clear cut presence of γ-MnOOH. In the light of Giovanoli's meticulous work [36] on the interconversions of δ-MnO_2 to γ-MnOOH, however, this may not be surprising. Giovanoli showed that thin plates of δ-MnO_2 were transformed, in a structurally guided reaction, into rafts or parallel needles of γ-MnOOH. Further, if the conversion of δ-MnO_2 to γ-MnOOH and then to Mn_3O_4 were to be the result of a dynamic equilibrium between Mn^{3+} ions in solution and γ-MnO_2 solid solution, then neither X-ray nor infrared spectra could be expected to reveal any specific features of γ-MnOOH. We might therefore conclude, if we dare conclude at all, that Sugimori's [20] hypothesis regarding the formation of δ-MnO_2 is not tenable. The suggestion of Holton *et al.* [21] seems to be more reliable in view of the X-ray and infrared data presented here. The 'aberrant' behaviour of CMD-1 could only be explained on the basis of K^+ ions present in the structure. At this stage of the argument we are unable to furnish any other reason for this behaviour of the discharge products of CMD-1.

To compare the infrared data of the final reduction products at $r \simeq 1$, $MnO_{1.52}$, we have also taken the spectral data of Mn_3O_4 prepared and characterized by us. The spectral data of almost all final products correspond well with the data of Mn_3O_4. So, the infrared data, at least, are unambiguous in this. The X-ray data at $r = 1$, which in many cases exhibit diagnostic δ-MnO_2 lines, are not corroborated by the infrared data. This again may be supportive of a dynamic equilibrium between Mn^{3+} ions in solution and γ-MnO_2 solid solution.

4. Conclusions

(i) The discharge capacities of chemical manganese dioxides (both CMD-1 and CMD-2) are found to be higher than those of electrolytic ones (both EMD and I.C.4).

(ii) Both CMDs and EMDs appear to follow similar reaction paths. There is practically no difference in their discharge products at $r = 1$, *i.e.*, at the end of the one-electron change. The reaction sequence seems to be

γ-MnO_2 ⟶ δ-MnO_2

$$\delta\text{-}MnO_2 + H_2O + e^- \longrightarrow MnOOH + OH^-$$

$$MnOOH + e^- \longrightarrow HMnO_2^-$$

$$2MnOOH + HMnO_2^- \longrightarrow Mn_3O_4 + H_2O + OH^-$$

(iii) Some intermediate reduction products of CMD, however, do not exhibit the diagnostic δ-MnO_2 peaks consistently. This could be due to a greater degree of disorder and dispersion in the intermediate δ-MnO_2 that is formed before Mn_3O_4 crystallizes out. The discharge mechanism of synthetic birnessite, commonly referred to as δ-MnO_2, vindicates the mechanism proposed by Holton and Tye for γ-MnO_2.

(iv) The clear appearance of a new phase beyond $r = 1$ is indicated by the discontinuity in the plots of the ratio of the cell volume to the degree of reduction as a function of the degree of reduction.

The plots of a''/a' *versus* r (Fig. 12) do not show any resemblance to the similar plots of γ/ϵ-MnO_2 in acidic/neutral electrolyte. (See Fig. 17.) No Jahn–Teller type of distortion seems to occur in alkaline electrolyte during the course of the discharge from $r = 0.5$ to $r = 1$.

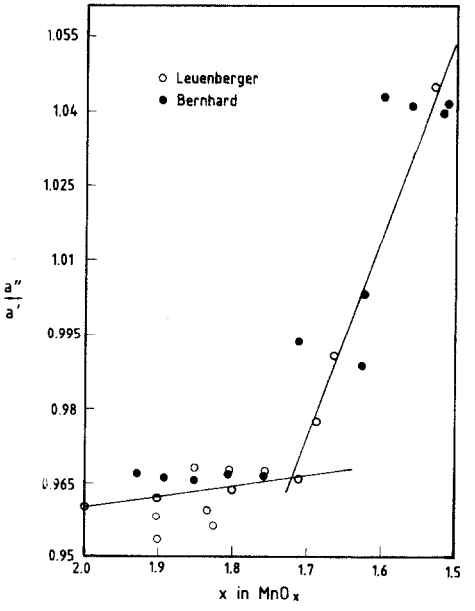

Fig. 17. Ratio of the octahedron cell edges *vs.* degree of reduction.

List of symbols

Å	Ångström unit
a, *b*, *c*	Crystal lattice parameters
mA	Milliampere

mA h	Milliampere hour
α	Alpha
γ	Gamma
δ	Delta
ρ	Rho
d	Interplanar distance
ZIA	Zinc ion adsorption
ASTM	American Society for Testing Materials
λ	Lambda
OCV	Open circuit voltage
CCV	Closed circuit voltage
CMD	Chemical manganese dioxide
EMD	Electrolytic manganese dioxide
r	Parameter for state of reduction

References

1 N. C. Cahoon and M. P. Korver, *J. Electrochem. Soc., 106* (1959) 745.
2 J. Brenet, P. Malleson and A. Grund, *C. R. Acad. Sci., 242* (1956) 111.
3 K. Neumann and W. Fink, *Z. Elektrochem., 62* (1958) 114.
4 J. P. Gabano, J. F. Laurent and B. Morignat, *Electrochim. Acta, 9* (1964) 1093.
5 G. S. Bell and R. Huber, *J. Electrochem. Soc., 111* (1964) 1.
6 A. Kozawa and J. F. Yeager, *J. Electrochem. Soc., 112* (1965) 959.
7 A. Kozawa and R. A. Powers, *J. Electrochem. Soc., 113* (1966) 870.
8 D. Boden, C. U. Venuto, D. Wisler and R. B. Wylie, *J. Electrochem. Soc., 114* (1967) 415.
9 J. McBreen, in D. H. Collins (ed.), *Power Sources 5*, Academic Press, London, 1975, p. 525.
10 J. McBreen, *Electrochim. Acta, 20* (1975) 221 - 225.
11 W. C. Maskell, J. A. E. Shaw and F. L. Tye, *Electrochim. Acta, 26* (1981) 1403.
12 W. C. Maskell, J. A. E. Shaw and F. L. Tye, *J. Power Sources, 8* (1982) 113 - 120.
13 W. Feitknecht, H. R. Oswald and U. Feitknecht-Steinmann, *Helv. Chim. Acta, 43* (1960) 1947.
14 H. Bode, A. Schmier and D. Bertdt, *Z. Elektrochem., 66* (1962) 586.
15 J. P. Gabano, B. Morignat, E. Fialdes, E. Emery and J. F. Laurent, *Z. Phys. Chem., 46* (1965) 359.
16 R. Giovanoli, K. Bernhard and W. Feitknecht, *Helv. Chim. Acta, 51* (1968) 355.
17 J. Ambrose and G. W. D. Briggs, *Electrochim. Acta, 16* (1971) 111.
18 F. L. Tye, in M. Barak (ed.), *Electrochemical Power Sources*, Peter Peregrinus Ltd., Stevenage, U.K., 1980, p. 50.
19 A. Kozawa and R. A. Powers, *J. Electrochem. Soc. Jpn., 37* (1969) 31.
20 M. Sugimori, in B. Schumn, H. M. Joseph and A. Kozawa (eds.), *Manganese Dioxide Symp., Tokyo*, Vol. 2, The Electrochemical Soc., Cleveland, OH, 1980, p. 443.
21 D. M. Holton, W. C. Maskell and F. L. Tye, Presented at *14th Int. Power Sources Symp., Brighton, 17 - 20 Sept., 1984.* (Pre-publication text pp. 1 - 20.)
22 F. L. Tye, Manganese dioxide electrodes theory and practice for electrochemical applications, Plenary lecture, *The Electrochemical Symp., New Orleans, LA, 10 - 12 Oct., 1984.* (Pre-publication text p. 17.)
23 J. B. Fernandes, B. D. Desai and V. N. Kamat Dalal, *Electrochim. Acta, 28* (1983) 309.

24 D. M. Holton and F. L. Tye, in B. Schumn, H. M. Joseph and A. Kozawa (eds.), *Manganese Dioxide Symp., Tokyo,* Vol. 2, The Electrochemical Soc., Cleveland, OH, 1980, p. 244.
25 P. Rueschi, *J. Electrochem. Soc., 131* (1984) 2739.
26 J. B. Fernandes, B. D. Desai and V. N. Kamat Dalal, *Electrochim. Acta, 29* (1984) 181.
27 Cited in S. U. Falk and A. J. Salkind (eds.), *Alkaline Storage Batteries,* Wiley, New York, 1969, p. 534.
28 R. Giovanoli, E. Stähli and W. Feitknecht, *Helv. Chim. Acta, 53* (1970) 453.
29 R. Giovanoli and E. Stähli, *Chimia, 24* (1970) 52.
30 A. Kozawa, in K. Kordesh (ed.), *Manganese Dioxide Batteries,* Vol. 1, Marcel Dekker, New York, 1974, p. 509.
31 R. Giovanoli, *Chimia, 23* (1969) 471.
32 R. Giovanoli and U. Leuenberger, *Helv. Chim. Acta, 52* (1969) 2344.
33 W. C. Maskell, J. E. A. Shaw and F. L. Tye, *Electrochim. Acta, 26* (1981) 1406.
34 R. M. Potter and G. R. Rossman, *Am. Mineral., 64* (1979) 1199 - 1216.
35 J. B. Fernandes, B. D. Desai and V. N. Kamat Dalal, *J. Appl. Electrochem., 15* (1985) 355.
36 R. Giovanoli, W. Feitknecht and F. Fischer, *Helv. Chim. Acta, 54* (1971) 1112.